COMPDYN 2025
10th ECCOMAS Thematic Conference on
Computational Methods in Structural Dynamics and Earthquake Engineering
M. Papadrakakis, M. Fragiadakis (eds.)
Rhodes Island, Greece, 15-18 June 2025

SEISMIC FRAGILITY ANALYSIS OF MASONRY BUILDINGS USING REAL AND SIMULATED GROUND MOTION RECORDS

Daniel Caicedo[1], **Shaghayegh Karimzadeh**[1], **Vasco Bernardo**[1], **and Paulo B. Lourenço**[1]

[1] University of Minho
Department of Civil Engineering, ISISE, Campus de Azurém 4800-058
Guimarães, Portugal.
{ dcaicedod, shaghkn, vbernardo, pbl }@civil.uminho.pt

Abstract

Past investigations have shown the sensitivity of masonry structures to record-to-record variability (aleatory uncertainty). In this regard, the selection of seismic input for performance-based assessment might be an issue in regions with a lack of recorded accelerograms characteristic of large-magnitude events, which can be solved by utilising simulated records. This paper examines the consistency of fragility functions of masonry archetypes using real and simulated signals as input for non-linear incremental dynamic analyses (IDAs). Structural models are developed based on representative archetypes and typologies of the residential building stock in Portugal. These buildings are modelled in OpenSees to consider In-Plane (IP) and Out-of-Plane (OOP) effects simultaneously while improving computational efficiency. Ground motion simulations are carried out using a stochastic finite-fault simulation approach that incorporates the dynamic corner frequency concept. Following this, two sets of records are independently selected, consisting of both real and simulated accelerograms. The real records are chosen to meet seismological compatibility criteria with the simulated data. Subsequently, IDAs are performed, and fragility curves are developed. The fragility obtained after real and simulated records are contrasted in terms of the moments of the distribution (median and dispersion). Finally, some practical recommendations are provided for the utilisation of simulated ground motions for performance assessment of masonry structures.

Keywords: Incremental dynamic analysis; Out-of-plane response; Real and simulated records; Record-to-record variability; Fragility curves.

1 INTRODUCTION

Historic urban centres in Europe are mostly composed of unreinforced masonry (URM) buildings that are highly vulnerable to earthquake damage. A large portion of the building stock located in regions of significant seismicity has been affected in the past by major earthquakes such as the Faial (1998) earthquake in Portugal [1], the L'Aquila (2009) and Emilia (2012) earthquakes in Italy, Lesvos (2017) in Greece [2–4], and recently the Kahramanmaraş Earthquakes of $M_w = 7.7$ and $M_w = 7.6$, in Türkiye [5]. One major challenge in the seismic assessment of URM is to account for multiple sources of epistemic and aleatory uncertainty. Ideally, both sources of uncertainty should be considered simultaneously. Nevertheless, accounting for both in the seismic assessment of historical masonry buildings can be extremely expensive from a computational standpoint. In this regard, Tomić et al. [6] analysed deeply the behaviour of historical masonry constructions accounting for the uncertainty stemming from material and modelling properties. Afterwards, the effect of record-to-record variability was studied through multiple-record incremental dynamic analyses (IDA) [7] and probabilistic seismic demand models (PSDM) [8] showing that the consideration of signal input uncertainty and modelling parameters variability led to nearly identical results in terms of capacity and fragility functions. However, accounting for this aleatory uncertainty faces the additional challenge of requiring for full time-series of ground motion records, which might be difficult in regions lacking seismic stations or a limited history of large magnitude and potentially destructive earthquakes.

Cutting-edge advances in ground motion simulations offer a potential solution to the issue of lacking earthquake motions by simulating acceleration time-series tailored to specific seismic hazard scenarios characterised by earthquake magnitude, source-to-site distance, and site conditions [9]. Simulation techniques can be categorised as deterministic source-based, stochastic sourced-based, stochastic site-based, and hybrid models [10]. Among all, stochastic methods are preferable in engineering applications due to their relative simplicity, ability to simulate broadband frequencies relevant to engineering structures, and straightforward calibration [11,12]. In the literature, several authors have calibrated and validated the use of stochastic simulations for developing ground motion models and assessing seismic demand of various engineering structures particularly reinforced concrete and steel structures [13–17]. Yet, the utilisation of simulated ground motions in the assessment of URM is still an ongoing filed of research. In this context, Hoveidae et al. [18] investigated seismic damage to a historic masonry monument in Tabriz, Iran, for different scenario earthquakes using stochastically simulated ground motion records. Karimzadeh et al. [19] compared source-based and site-based stochastic simulation approaches in the assessment of monumental masonry structures. Lastly, Bernardo et al. [20] conducted the fragility-based assessment of traditional masonry buildings in Portugal using simulated ground-motion records.

This study examines the consistency of fragility functions of URM archetypes using real and simulated signals as input for non-linear IDAs. Ground motion simulations are generated through the stochastic finite-fault method which is based on a dynamic corner frequency approach [21]. A numerical case study representative of masonry typologies in Portugal is modelled in OpenSees [22] using 3-dimensional macroelements that account for in-plane (IP) and out-of-place (OOP) effects of masonry walls [23]. A first suite of real motions consistent with the variability of European hazard is selected. Subsequently, a set of simulated records is selected following the same seismological criteria and matching the mean response spectra of the first set. Both sets are used as input for IDAs from which capacity and fragility curves are derived. The median and dispersion of the fragility functions are employed as metrics to compare the performance of both sets of records. The objective is to investigate the application of previously generated and validated simulated ground motion datasets, as referenced in the

literature [24,25], for the seismic evaluation of URM structures. The paper is organised as follows. Section 2 presents the definition of the numerical case study and finite element macro-modelling implementation. Section 3 provides a description of the ground motion selection approach for real and simulated time-series. The discussion of the results in terms of failure characterisation, and capacity and fragility functions, is presented in Section 4. Finally, section 5 delivers some relevant conclusions from the study.

2 CASE STUDY DEFINITION

A representative archetype of URM constructions is taken from the portfolio presented in Bernardo et al. [26] of typical pre-code masonry buildings in the Metropolitan Area of Lisbon. As in the original reference, the building model is denoted as B2_3P. The following sub-sections briefly describe the buildings' topology and the modelling approach.

2.1 Building archetype

The B2_3P model resembles a 3-storey URM building of regular plan with dimensions of 12.50 m × 12.50 m. The storey height is 3.00 m. The wall thicknesses are 45 cm in the direction of the main façade (See Figure 1) and 30 cm in the perpendicular direction. Wall and spandrels thicknesses are 60 cm and 30 cm, respectively. Additionally, thinner partitions ranging from 15 to 25 cm, can be found as part of the interior configuration. The timber floors are constituted by timber sheathing and timber joists perpendicular to the facades. Table 1 summarises the description of the building topology.

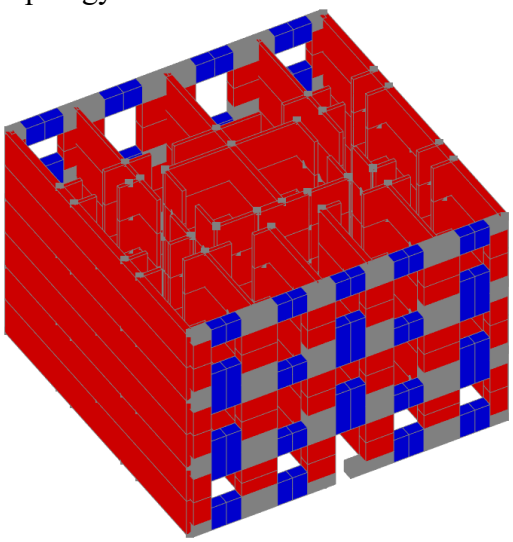

Figure 1: B2_3P typology.

Table 1: Description of the building topology.

Building	b2_3p
General	typical pre-code URM building
Nº stories	3
Dimensions in plan	12.50 m × 12.50 m
Storey height	3.00 m
Wall thickness	45 − 30 cm
Internal partitions	15 − 25 cm
Floor system	timber sheathing and timber joists

2.2 Modelling approach

The three-dimensional macroelement formulation introduced by Vanin et al [23] for modelling the IP and OOP response of masonry walls is adopted for the large-scale representation of the building. The macroelement is available in the OpenSees library [22] and it is formulated as a one-dimensional element with two nodes at the element ends and one additional node at the midspan. The macroelement is able to capture the IP and OOP response through three sectional models applied at the element ends and at the central section which can reproduce deformation across the main axes. Furthermore, P-Δ formulation is considered to capture the nonlinear geometrical effects. Considering the rotations and lumped shear deformations at the central node, drift values can be calculated individually for flexural and shear deformations. Exceeding the limits in drift values will lead to the loss of lateral strength of the element.

Timber floors are idealised as flexible diaphragms and modelled using orthotropic elastic membranes with higher stiffness in the direction of the beam span, and a lower stiffness in the other direction. The membrane definition is given by the two moduli of elasticity in the orthogonal directions, shear modulus, and thickness of the diaphragm (i.e., E_x, E_y, G_{xy}, and t_f, respectively). Although the floors are assumed as linear elastic, the floor-to-wall connections are modelled to account for non-linear behaviour and potential connection failure that can result in the OOP failure of a pier element (i.e., partial or total overturning of the façade [27]). To this aim, zero-length elements are used to model the frictional interfaces and possible relative displacement between the nodes, in which frictional sliding is allowed in the perpendicular direction to the wall while pounding of the beam towards the walls can occur in the opposite direction. Masonry material and modelling parameters are reported in Table 2.

Table 2: Material and modelling parameters.

Parameter	Unit	Definition	Adopted value
		Masonry Parameters	
E_m	[Pa]	Modulus of elasticity	4.00×10^9
G_m	[Pa]	Shear modulus	1.70×10^9
f'_{cm}	[Pa]	Compressive strength	5.00×10^6
c_m	[Pa]	Cohesion	0.15×10^6
μ_m	[-]	Friction coefficient	0.80
ρ	[kg]	Density	1800
		Modelling Parameters	
$\delta_{c,flexure}$	[-]	Drift capacity in flexure	0.01035
$\delta_{c,shear}$	[-]	Drift capacity in Shear	0.007
ζ	[-]	Damping ratio	0.05

3 GROUND MOTION SELECTION

Two independent suites of motions (i.e., real and simulations) are selected for comparison purposes and to dig into the implementation of stochastic ground motion simulations in the seismic analysis of masonry constructions. The following sub-sections describe the selection approach for real and simulated motions, respectively.

3.1 Real Accelerograms

Jayaram et al. [28] methodology is adopted to collect a set of 21 accelerograms covering the hazard of the most relevant seismic-prone areas in Europe (i.e., Italy, Greece, Turkey, Portugal, etc.). These ground motions are selected based on pre-defined hazard scenarios, that is, $4.5 \leq$

$M_w \leq 7.8$; 145 m/s $\leq V_{s30} \leq$ 960 m/s; $R_{JB} \leq$ 180 km, and no pulse-like records. Figure 2 shows the 5% damped geometric mean spectral acceleration (S_a) of the selected records, alongside the mean, median, and 95% confidence interval. It is noted that, to maintain consistency with the stochastic simulation output, which represents a random horizontal motion component, only one horizontal component from each event is selected.

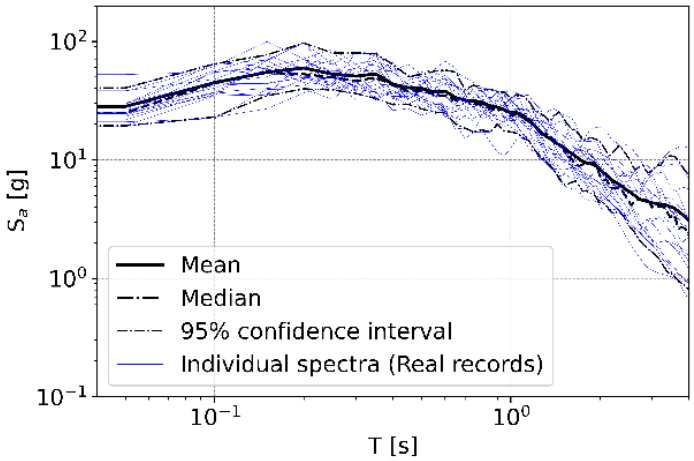

Figure 2: 5% damped geometric mean S_a of real records.

3.2 Simulated accelerograms

The same seismological criteria, as with the real records, is considered for the selection of the simulated time-series. Those simulations have been generated using the stochastic source-based approach better-known in the literature as stochastic finite-fault ground motion simulation methodology through a dynamic corner frequency algorithm [11,21]. This study utilises a validated simulated dataset previously developed by the authors in Türkiye and Iran. For further details, refer to [24,25]. The selection approach of simulations targets the mean response spectra of the real suite of motions, in such a way that a clear reduction in the scatter of S_a ordinates is achieved (See Figure 3). Table 3 reports both, real and simulated motions, selected as input for the dynamic analyses, including values of M_w, V_{s30}, R_{JB}, and PGA.

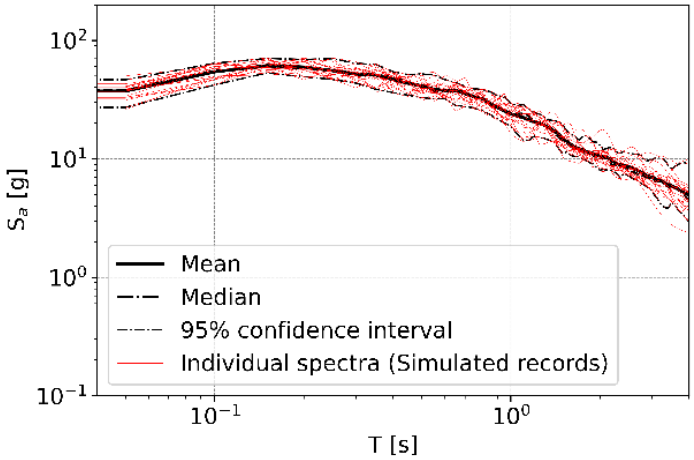

Figure 3: 5% damped geometric mean S_a of simulated records.

Table 3: Real and simulated motions selected for dynamic analyses

Filename	Event ID	M_w	V_{S30} (m/s)	R_{JB} (km)	PGA (m/s^2)
Real records					
TK.3805.HNX.D.INT-20230206_0000008.ACC.MP.ASC	INT-20230206_0000008	7.8	384	175.45	23.32
HI.NAX1.HNX.D.EMSC-20201030_0000082.ACC.MP.ASC	EMSC-20201030_0000082	7.0	461	134.88	30.32
IT.AQK.00.HGX.D.EMSC-20170118_0000034.ACC.MP.ASC	EMSC-20170118_0000034	5.5	705	14.56	21.52
IT.SDM.00.HGX.D.EMSC-20160824_0000006.ACC.MP.ASC	EMSC-20160824_0000006	6.0	752	45.23	23.08
IT.SSU.00.HNX.D.IT-2012-0011.ACC.MP.ASC	IT-2012-0011	6.0	489	38.90	17.11
IT.TRL.00.HGX.D.EMSC-20161026_0000095.ACC.MP.ASC	EMSC-20161026_0000095	5.9	380	45.04	18.99
IT.ASG.00.HNX.D.IT-1976-0002.ACC.MP.ASC	IT-1976-0002	6.4	960	127.85	21.78
IT.TRL.00.HGX.D.EMSC-20160824_0000013.ACC.MP.ASC	EMSC-20160824_0000013	5.5	380	39.15	21.43
IT.CLF.00.HNX.D.IT-1997-0105.ACC.MP.ASC	IT-1997-0105	4.5	145	3.24	32.16
TK.1801.00.HNX.D.TK-2000-0258.ACC.MP.ASC	TK-2000-0258	5.0	348	9.04	18.79
IT.AQK.00.HNX.D.IT-2009-0174.ACC.MP.ASC	IT-2009-0174	5.0	705	15.41	16.03
IT.MDN.00.HNX.D.IT-2012-0010.ACC.MP.ASC	IT-2012-0010	5.5	213	23.49	18.37
HI.VAS2.HNX.D.EMSC-20151120_0000014.ACC.MP.ASC	EMSC-20151120_0000014	4.7	261	19.50	26.93
IT.NRN.00.HGX.D.EMSC-20161030_0000029.ACC.MP.ASC	EMSC-20161030_0000029	6.6	811	59.17	18.28
IT.NOR.00.HGX.D.EMSC-20170118_0000119.ACC.MP.ASC	EMSC-20170118_0000119	5.0	423	36.51	19.62
TK.3116.HNX.D.INT-20230206_0000222.ACC.MP.ASC	INT-20230206_0000222	7.5	870	167.65	19.13
IT.GBP.00.HNX.D.IT-1998-0063.ACC.MP.ASC	IT-1998-0063	4.8	224	20.11	22.78
IT.CSC.00.HNX.D.IT-1997-0004.ACC.MP.ASC	IT-1997-0004	5.7	698	27.34	25.97
IT.MTR.00.HNX.D.IT-2009-0102.ACC.MP.ASC	IT-2009-0102	5.5	689	27.96	24.07
IT.GBP.00.HGX.D.EMSC-20161026_0000077.ACC.MP.ASC	EMSC-20161026_0000077	5.5	224	62.30	23.34
IT.NRC.00.HNX.D.IT-1997-0091.ACC.MP.ASC	IT-1997-0091	5.4	498	28.95	22.23
Simulated records					
Tabriz14-9-18	6.8-38.078-46.396	6.8	310	57.12	25.07
Tabriz13-14-5	7.1-38.078-46.224	7.1	310	62.95	23.72
Tabriz13-9-8	6.8-38.078-46.258	6.8	310	56.04	27.12
Tabriz1-7-2	6.8-38.078-46.189	6.8	310	59.60	27.65
Tabriz1-8-5	6.8-38.078-46.224	6.8	310	61.67	28.63
Tabriz13-9-9	6.8-38.042-46.258	6.8	310	54.89	29.01
Tabriz13-14-3	7.1-38.042-46.189	7.1	310	64.76	26.29
Tabriz1-8-7	6.8-38.113-46.258	6.8	310	61.12	29.39
VanM71SoilGS_Set1_acc_s130	7.1-130	7.1	310	75.86	22.50
Tabriz13-28-1	7.1-38.113-46.189	7.1	310	67.16	25.78
Tabriz13-1-11	6.8-38.078-46.293	6.8	310	53.14	27.89
AfyonM6SoilD_Set1_acc_s083	Jun-83	6.0	255	81.64	25.19
Tabriz1-16-3	6.8-38.042-46.189	6.8	310	62.63	27.06
Tabriz14-9-20	6.8-38.007-46.396	6.8	310	54.24	29.66
Tabriz2-8-16	6.8-38.078-46.361	6.8	310	58.32	27.75
Tabriz2-14-17	6.8-38.042-46.361	6.8	310	61.01	27.99
AfyonM58SoilD_Set1_acc_s012	5.8-12	5.8	255	66.92	24.09
duzceM7SiteD_acc_s009	9-Jul	7.0	255	91.33	21.69
Tabriz13-28-2	7.1-38.078-46.189	7.1	310	65.87	27.86
VanM71SoilGS_Set1_acc_s032	7.1-32	7.1	310	85.12	29.12
Tabriz1-4-21	6.8-38.042-46.43	6.8	310	77.67	27.58

4 ANALYSIS OF RESULTS

This section compares the performance of both sets of records in the IDA of the numerical case study. The discussion is organised in terms of failure analysis and the distribution observed within the capacity and fragility functions derived from IDAs.

4.1 Failure characterisation

Each suite of motions provided the seismic input for 210 analyses, with bins of shaking intensity, in terms of g, distributed as [0.05 0.10 0.15 0.20 0.25 0.30 0.35 0.40 0.45 0.50]. Since simulations from the stochastic approach employed herein represent only a random horizontal component of the earthquake (See section 3), for both real and simulated records, the seismic input of non-linear analyses is applied in the direction parallel to the main façade of the building (x-dir) which is also the weakest axis of the building. This assumption supposes a fair comparison between real and simulated input motions and their effects on structural behaviour. For the real recordings, 91 collapse cases out of 210 analyses were observed, denoting, in this case, approximately 43% of failure observations. On the other hand, 95 analyses led to the global collapse of the building (i.e., 45%) when simulated record datasets were employed as input motions. For both real and simulated sets, 5% of all observations correspond to IP failures while the rest are OOP. In that regard, 81 out of 210 analyses correspond to OOP failures for the real records while 84 out of 210 analyses induced OOP failures for the simulated ones, that is 39% and 40% for real and simulated sets, respectively (See Figure 4). The classification of IP failures shows also consistency for both suites of motions as depicted in Figure 5. Within both sets, no shear failures were observed, only 1 case corresponds to flexure IP failure while the rest are mixed IP failures (i.e., approximately the same number of piers exceed the $\delta_{c,flexure}$ and $\delta_{c,shear}$ limits). Lastly, the failure location is shown in Figure 6. Most of the IP failures correspond to mixed locations while the single flexure IP was located at 3rd storey in the "x" axis direction (F3 x-dir). As expected, OOP failures are found at upper stories [7,29], F3 x-dir and F2 x-dir, with just a minimal portion at F1 x-dir.

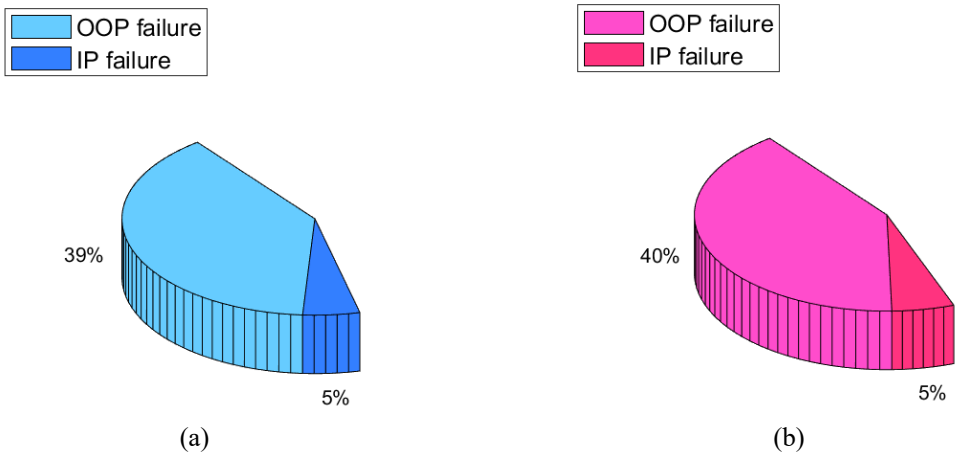

(a) (b)

Figure 4: Distribution of IP and OOP observations for (a) real records and (b) simulated records.

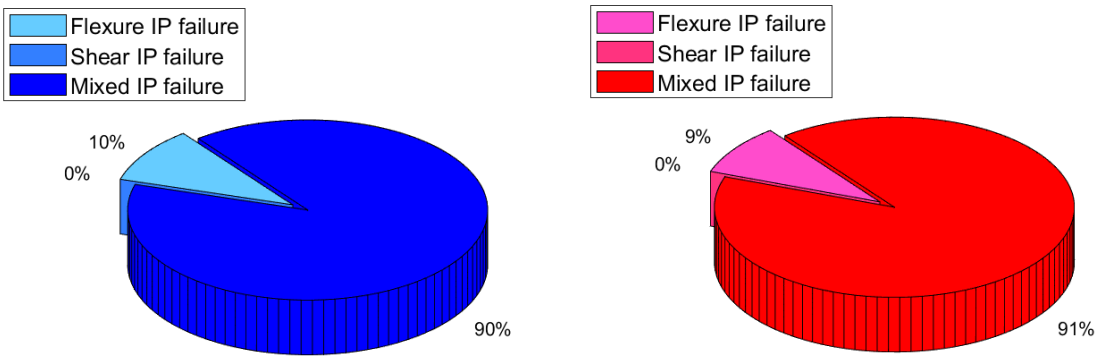

(a) (b)

Figure 5: Classification of IP failures for (a) real records and (b) simulated records.

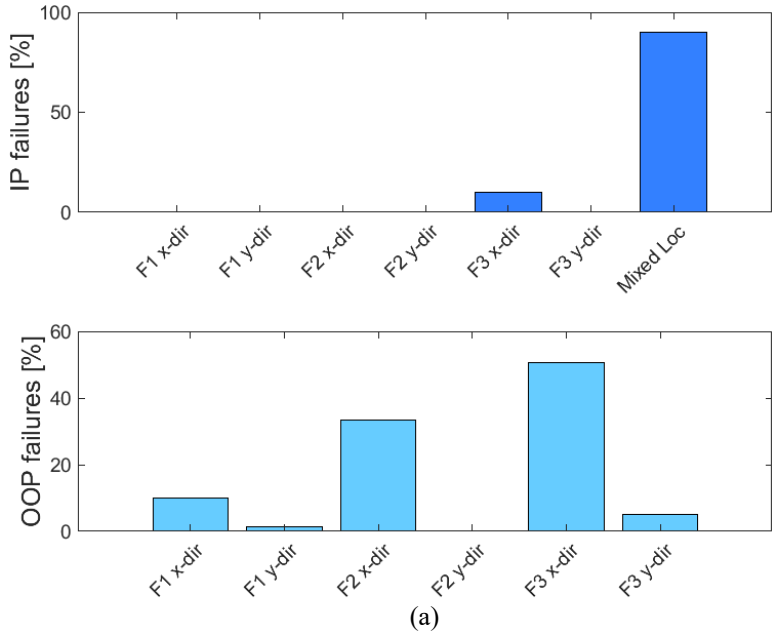

(a)

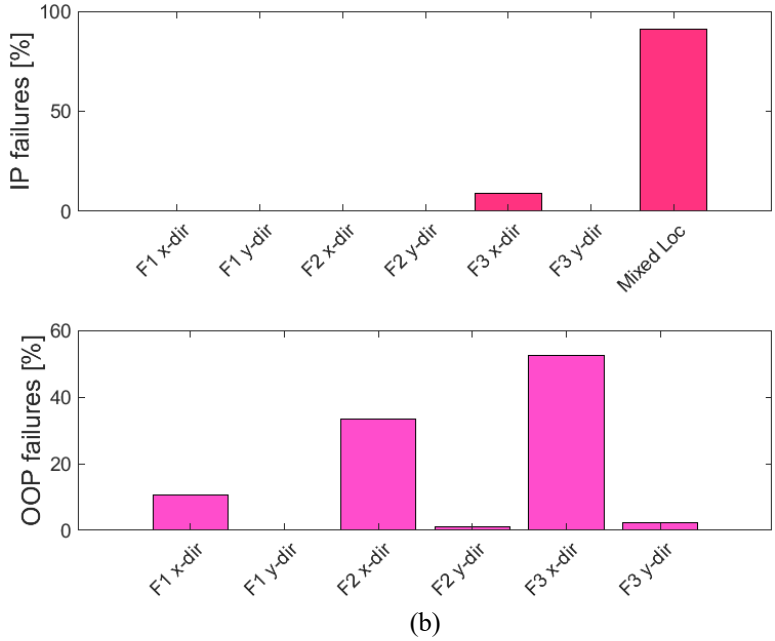

(b)

Figure 6: Failure localisation for (a) real records and (b) simulated records.

4.2 Capacity and fragility analysis

After conducting non-linear time-history analyses, the IDA curves are derived. Figure 7 (a) and (b) show the IDA curves, performance points of immediate occupancy (IO) and collapse prevention (CP) [7], and assuming the maximum global drift ratio as EDP, for real and simulated records, respectively. The 16th, 50th, and 84th percentiles can be calculated from these results, among which the 50th fractile corresponds to the median capacity for the structure under analysis. The performance of both sets is compared in Figure 8 in terms of the capacity of the structure. Both curves show perfect correspondence in the elastic range while a slightly lower capacity is attained with the simulated records. This conservative trend is expected after observing more collapse cases for the simulated suite of motions, as discussed in section 4.1.

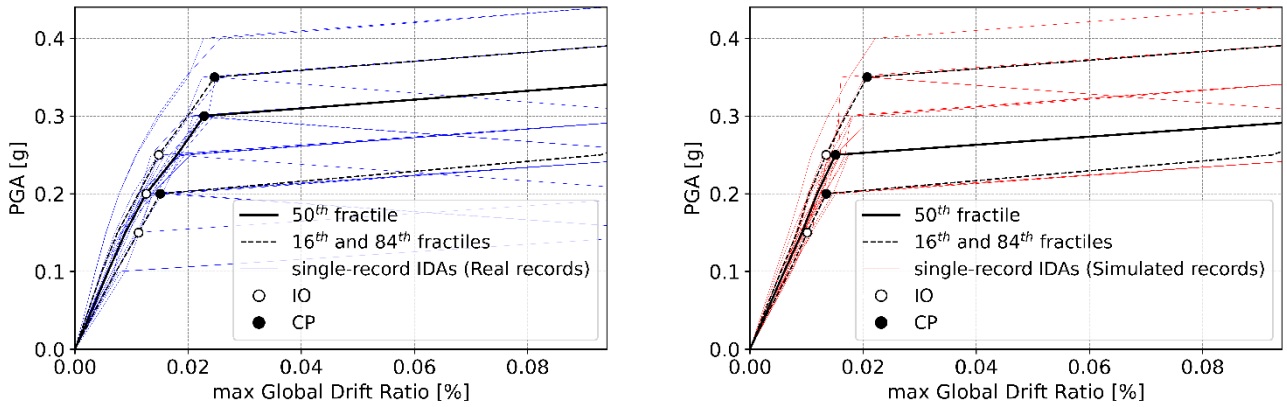

Figure 7: IDA curves displaying maximum values of EDPs for (a) real records and (b) simulated records.

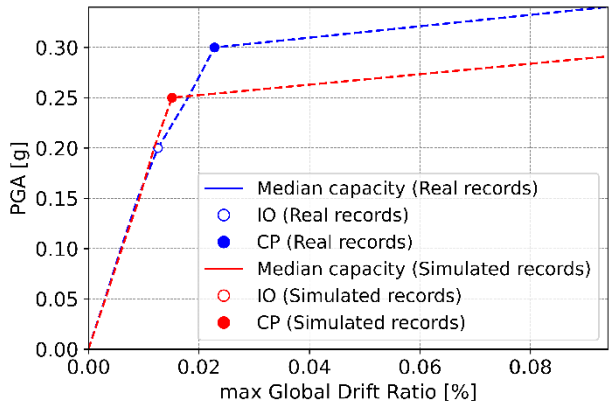

Figure 8: Median capacity curves.

Next, by considering the ratio of the number of records that caused structural collapse to the total number of records at a ground shaking intensity level, a fragility function at collapse stage can be calculated. Such analytical curves, shown in Figure 9, are derived simply by fitting lognormal cumulative distribution (LogCDF) to the collapse observations. The values of median and dispersion, $\hat{\eta}$ and $\hat{\beta}$, are shown within the plot for the case of real records and simulations. It is observed how the effect of lower dispersion in the selection and IDAs of simulated records has a direct impact in reducing logarithmic standard deviation in the fitting process, i.e., $\hat{\beta} = 0.0557$. Both functions are compared in Figure 10. Although similar, the simulated records lead to more conservative estimations in the likelihood of failure occurrence, which is again consistent the observations made from IDAs.

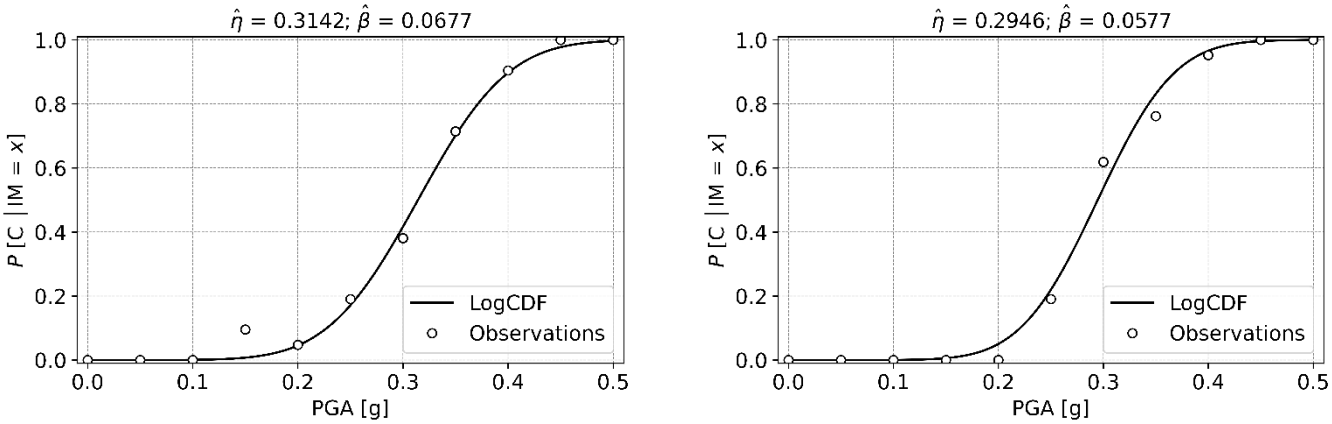

(a) Real records (b) Stochastic simulations

Figure 9: Fitting of analytical collapse fragility functions.

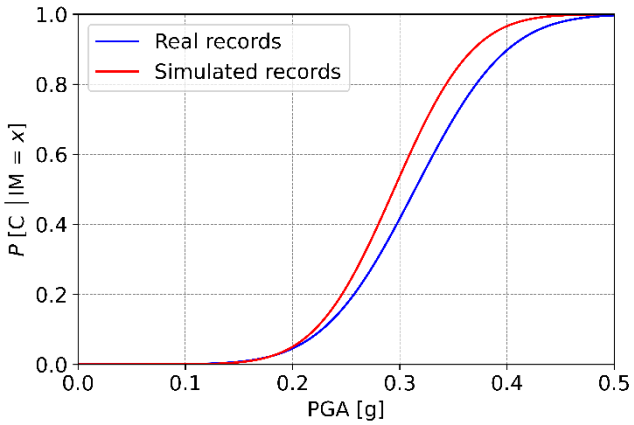

Figure 10: Comparison of analytical fragility.

5 CONCLUSIONS

The implementation of stochastic ground motion simulations for the collapse fragility analysis of masonry buildings was explored in this paper. Those simulations are taken from the literature [24,25] generated through the stochastic finite-fault methodology by [11,21]. The masonry archetype B2_3P from the portfolio [26] was adopted as case study. This building was modelled in OpenSees [22] using 3-dimensional macroelements [23] to account for in-plane (IP) and out-of-place (OOP) mechanisms. As a reference for comparison, real motions were selected based on pre-defined hazard scenarios. Subsequently, ground motion simulations were selected assuming the same seismological criteria and targeting the mean response spectra of the real suite of motions. Following this, IDAs were performed. The comparison in terms of failure characterization showed good agreement in the distribution of IP and OOP observations, classification of IP failures, and location of failure for both sets of real accelerograms and stochastic simulations. Further, the consistency of capacity and fragility functions was examined, leading the simulated set to slightly more conservative results than the real suite of motions. It was observed how the effect of dispersion in the ground motion selection approach and IDAs has a direct impact on the numerical fitting of the $\hat{\eta}$ and $\hat{\beta}$ values to the statistical distribution. The promising results demonstrate the effectiveness of simulated records, generated through stochastic finite-fault approaches, in their application to the risk analysis of URM buildings. Thus, the findings of this work are promising, and future works should consider more case

studies as well as analysing deeply the outcomes of probabilistic assessments for the purpose of validation.

ACKNOWLEDGMENT

This study has been partly funded by the STAND4HERITAGE project that has received funding from the European Research Council (ERC) under the European Union's Horizon 2020 research and innovation program (Grant agreement No. 833123), as an Advanced Grant. This work was also partly financed by FCT / MCTES through national funds (PIDDAC) under the R&D Unit Institute for Sustainability and Innovation in Structural Engineering (ISISE), under reference UIDB / 04029/2020 (doi.org/10.54499/UIDB/04029/2020), and under the Associate Laboratory Advanced Production and Intelligent Systems ARISE under reference LA/P/0112/2020. This work is partly financed by national funds through FCT - Foundation for Science and Technology, under grant agreement 2023.01101.BD attributed to the first author.

REFERENCES

[1] Karimzadeh S, Funari MF, Szabó S, Hussaini SMS, Rezaeian S, Lourenço PB. Stochastic simulation of earthquake ground motions for the seismic assessment of monumental masonry structures: Source-based vs site-based approaches. Earthq Eng Struct Dyn 2023.

[2] Calderoni B, Cordasco EA, Del Zoppo M, Prota A. Damage assessment of modern masonry buildings after the L'Aquila earthquake. Bulletin of Earthquake Engineering 2020;18. https://doi.org/10.1007/s10518-020-00784-5.

[3] Penna A, Morandi P, Rota M, Manzini CF, da Porto F, Magenes G. Performance of masonry buildings during the Emilia 2012 earthquake. Bulletin of Earthquake Engineering 2014;12. https://doi.org/10.1007/s10518-013-9496-6.

[4] Vlachakis G, Vlachaki E, Lourenço PB. Learning from failure: Damage and failure of masonry structures, after the 2017 Lesvos earthquake (Greece). Eng Fail Anal 2020;117. https://doi.org/10.1016/j.engfailanal.2020.104803.

[5] Nasery MM, Çelik M, Şadoğlu E. Damage assessment of Siverek Castle during the Kahramanmaraş Earthquakes (Mw 7.7 and Mw 7.6) on 06 February 2023: Remediation and strengthening proposals. Eng Geol 2024:107511.

[6] Tomić I, Vanin F, Beyer K. Uncertainties in the seismic assessment of historical masonry buildings. Applied Sciences 2021;11:2280.

[7] Caicedo D, Tomić I, Karimzadeh S, Bernardo V, Beyer K, Lourenço PB. Collapse fragility analysis of historical masonry buildings considering in-plane and out-of-plane response of masonry walls. Eng Struct 2024;319:118804.

[8] Caicedo D, Tomić I, Karimzadeh S, Bernardo V, Beyer K, Lourenço PB. Optimal intensity measure and probabilistic seismic demand model for the assessment of historical masonry buildings considering in-plane and out-of-plane response. Manuscript Submitted for Publication to Reliability Engineering & System Safety 2024.

[9] Rezaeian S, Stewart JP, Luco N, Goulet CA. Findings from a decade of ground motion simulation validation research and a path forward. Earthquake Spectra 2024;40:346–78.

[10] Rezaeian S, Xiaodan S. Stochastic ground motion simulation 2014.

[11] Atkinson GM, Assatourians K. Implementation and validation of EXSIM (a stochastic finite-fault ground-motion simulation algorithm) on the SCEC broadband platform. Seismological Research Letters 2015;86. https://doi.org/10.1785/0220140097.

[12] Assatourians K, Atkinson G. EXSIM12: a stochastic finite-fault computer program in FORTRAN 2012.

[13] Pang R, Chen K, Fan Q, Xu B. Stochastic ground motion simulation and seismic damage performance assessment of a 3-D subway station structure based on stochastic dynamic and probabilistic analysis. Tunnelling and Underground Space Technology 2022;126:104568.

[14] Ozsarac V, Karimzadeh S, Askan A, Erberik MA. Seismic demands of bare and base-isolated steel frames for real against simulated records of a past earthquake. Structure and Infrastructure Engineering 2022;18:1266–81.
[15] Hu H, Gan G, Bao Y, Guo X, Xiong M, Han X, et al. Nonlinear stochastic seismic response analysis of three-dimensional reinforced concrete piles. Buildings 2023;13:89.
[16] Askan A, Altindal A, Aydin MF, Erberik MA, Koçkar MK, Tun M, et al. Assessment of urban seismic resilience of a town in Eastern Turkiye: Turkoglu, Kahramanmaras before and after 6 February 2023 M 7.8 Kahramanmaras earthquake. Earthquake Spectra 2024:87552930241274720.
[17] Karimzadeh S, Mohammadi A, Salahuddin U, Carvalho A, Lourenço PB. Backbone ground motion model through simulated records and XGBoost machine learning algorithm: An application for the Azores plateau (Portugal). Earthq Eng Struct Dyn 2023. https://doi.org/https://doi.org/10.1002/eqe.4040.
[18] Hoveidae N, Fathi A, Karimzadeh S. Seismic damage assessment of a historic masonry building under simulated scenario earthquakes: A case study for Arge-Tabriz. Soil Dynamics and Earthquake Engineering 2021;147. https://doi.org/10.1016/j.soildyn.2021.106732.
[19] Karimzadeh S, Funari MF, Szabó S, Hussaini SMS, Rezaeian S, Lourenço PB. Stochastic simulation of earthquake ground motions for the seismic assessment of monumental masonry structures: Source-based vs site-based approaches. Earthq Eng Struct Dyn 2023. https://doi.org/https://doi.org/10.1002/eqe.4012.
[20] Bernardo V, Karimzadeh S, Caicedo D, Hussaini SMS, Lourenço PB. Fragility-based seismic assessment of traditional masonry buildings on Azores (Portugal) using simulated ground-motion records. Earthquake Spectra 2024;40:2836–61.
[21] Motazedian D, Atkinson GM. Stochastic finite-fault modeling based on a dynamic corner frequency. Bulletin of the Seismological Society of America 2005;95. https://doi.org/10.1785/0120030207.
[22] McKenna F. OpenSees: a framework for earthquake engineering simulation. Comput Sci Eng 2011;13:58–66.
[23] Vanin F, Penna A, Beyer K. A three-dimensional macroelement for modelling the in-plane and out-of-plane response of masonry walls. Earthq Eng Struct Dyn 2020;49. https://doi.org/10.1002/eqe.3277.
[24] Temiz C, Hussaini SMS, Karimzadeh S, Askan A, Lourenço PB. Seismic scenario simulation and ANN-based ground motion model development on the North Tabriz Fault in Northwest Iran. J Seismol 2024:1–23.
[25] Karimzadeh S, Mohammadi A, Hussaini SMS, Caicedo D, Askan A, Lourenço PB. ANN-Based Ground Motion Model for Turkey using Stochastic Simulation of Earthquakes. Geophys J Int 2023:ggad432.
[26] Bernardo V, Campos Costa A, Candeias P, Costa A. Seismic vulnerability assessment and fragility analysis of pre-code masonry buildings in Portugal. Bulletin of Earthquake Engineering 2022;20:6229–65.
[27] Nale M, Minghini F, Chiozzi A, Tralli A. Fragility functions for local failure mechanisms in unreinforced masonry buildings: a typological study in Ferrara, Italy. Bulletin of Earthquake Engineering 2021;19. https://doi.org/10.1007/s10518-021-01199-6.
[28] Jayaram N, Lin T, Baker JW. A Computationally efficient ground-motion selection algorithm for matching a target response spectrum mean and variance. Earthquake Spectra 2011;27. https://doi.org/10.1193/1.3608002.
[29] Costa AA, Penna A, Arêde A, Costa A. Simulation of masonry out-of-plane failure modes by multi-body dynamics. Earthq Eng Struct Dyn 2015;44. https://doi.org/10.1002/eqe.2596.